Numerical study of a laser generated cavitation bubble based on FVM and CLSVOF method

Numerical study of a laser generated cavitation bubble based on FVM and CLSVOF method

Jianyong Yin[1,2] **,Yongxue Zhang**[1,2] **and Yuning Zhang**[1,2,3]

[1]College of Mechanical and Transportation Engineering, China University of Petroleum-Beijing, Beijing 102249, China
[2]Beijing Key Laboratory of Process Fluid Filtration and Separation, China University of Petroleum-Beijing, Beijing 102249, China

[3]Email of the Corresponding Author: ZYNLZYN.100@163.COM

Abstract. Based on the open source software OpenFOAM, the finite volume method (FVM) is applied for discretization of the Navier-Stokes equation. A coupled level set and volume of fluid (CLSVOF) method is established to track the movement of the gas-liquid interface, for improving the accuracy of the simulation of interface curvature and surface tension force. The spherical collapse of a laser generated bubble in water is modeled with the consideration of viscosity, compressibility of both the gas and the liquid, and the surface tension of the liquid. The variations of the bubble radius during collapse predicted by the CLSVOF method are compared with the Gilmore model, the VOF method, which are more consistent with the experimental results. The velocity and the pressure around the bubble are also investigated. And the shock waves emitted by the bubble during the process are illustrated.

1. Introduction

Cavitation bubble is widely observed in practice and intensely investigated by many researchers due to its erosion effects in fluid machineries, for instance, in ship propellers [1], in turbines [2] and cryogenic pumps [3]. Theoretical study of the bubble dynamics started from Sir Rayleigh [4], who proposed a model, i.e, Rayleigh model, with the consideration of incompressible, inviscid and irrotational flow assumptions in infinite liquid. The model was extended by Plesset [5] with the consideration of surface tension and viscosity of the liquid, which was named as Rayleigh-Plesset model. Other important works, e.g. Gilmore [6] enhanced the model with the compressibility effects.

Many numerical methods have been developed to simulate the cavitation bubble dynamics, e.g. the boundary integral method (BIM) [7-10] and the finite volume method (FVM) [11-13]. BIM is widely applied to investigate the bubble dynamics because of its high computational efficiency [10]. However, it's difficult to simulate the change of topology when the bubbles disintegrate into separate parts [14]. Meanwhile, there are also problems for the investigation on the coalescence phenomenon [15]. Compared with BIM, FVM is rather unproblematic change of topology of the bubble and is used in this paper. Both Level Set (LS) method [16, 17] and Volume of Fluid (VOF) method [12, 18] are widely applied to track the movement of the gas-liquid interface. The LS method with sharp interface capturing couldn't preserve mass conservation due to the re-distancing process [19]. The VOF method is mass conservative, while it is smearing of interface where the surface tension is dominant, especially. To take advantages of both the mass conservation of the VOF method and the sharp interface capturing of the LS method, Sussman [20] implemented a coupled LS and VOF (CLSVOF) method for computing the growth and collapse of vapor bubble, assuming that the liquid was incompressible and the vapor was a constant pressure in space.

In the present work, the open source software OpenFOAM [21] based on FVM method is used for studying the cavitation bubble. The CLSVOF method is applied for capturing the gas-liquid interface. The paper is organized as follows. The numerical methodology is well described in section 2. The initial conditions for numerical simulation are setup and explained in section 3. In section 4, both the qualitative and quantitative comparisons among the results predicted by Gilmore model, the VOF method, the CLSVOF method and the experimental results are presented. The emission and propagation of shock wave from the cavitation bubble collapse in infinite field is illustrated. Some new phenomena are also found and discussed. Finally, the conclusions are made in section 5.

2. Numerical methodology

In the section, the governing equations implemented in OpenFOAM for the compressible two-phase flow are presented, including the continuity equation, momentum equation, equations of state for gas phase and liquid phase and VOF equation. Meanwhile, a theoretical formulation of the CLSVOF method is also presented. The phase change and heat transfer are ignored due to their complexity for computing strong collapses. Koch et al. [12] found that reasonably accurate results still could be obtained even without the considerations of phase change and heat transfer. Without phase change, the bubble is considered to be filled with non-condensable gas and the saturated vapor pressure is set to be zero [22]. In CLSVOF, the VOF equation is solved to ensure mass conservative. An initial value of the LS function is defined from the VOF equation, and then, a re-initialization is performed to obtain the signed distance function [23]. The goal of coupling the LS and VOF is to improve the accuracy of the simulation of interface curvature and surface tension force. The governing equations for the numerical simulation are given below:

Continuity equation:

$$\frac{\partial \rho}{\partial t} + \nabla \cdot \left(\rho \boldsymbol{U} \right) = 0 \tag{1}$$

The continuity equation for each of the phases is:

$$\frac{\partial(\alpha_i\rho_i)}{\partial t}+\nabla\cdot(\alpha_i\rho_i\boldsymbol{U})=0 \qquad (i=l,g) \tag{2}$$

Here, $\boldsymbol{U}$ is the velocity vector; t is time variable; α_i is the volume fraction. And the α_l and α_g are introduced to represent the volume fraction of liquid (l) phase and gas (g) phase, respectively, which obey the algebraic relationship ($\alpha_l+\alpha_g=1$) with $\alpha_l=1$ in the liquid phase and $\alpha_g=1$ in the gas phase; ρ is the average density determined by $\rho=\alpha_l\rho_l+\alpha_g\rho_g$.

Momentum equation:

$$\frac{\partial(\rho\boldsymbol{U})}{\partial t}+\nabla\cdot(\rho\boldsymbol{U}\boldsymbol{U})=-\nabla p+\nabla\cdot\boldsymbol{T}+\rho\boldsymbol{g}+\int_{S(t)}\sigma\kappa(\boldsymbol{x}')\boldsymbol{n}(\boldsymbol{x}')\delta(\boldsymbol{x}-\boldsymbol{x}')dS' \tag{3}$$

Here, p is the pressure field; $\boldsymbol{g}$ is the gravitational acceleration; the fourth term on the right side is the surface force acting at the gas-liquid interface; σ is the surface tension coefficient; κ is twice the mean curvature of the interface; $\boldsymbol{n}$ is the unit normal to the interface; δ is the Dirac delta function,; S(t) is the gas-liquid interface; $\boldsymbol{x}$` is a point on the interface; and $\boldsymbol{x}$ is the point at which the equation is solved; $\boldsymbol{T}$ is the viscous stress tensor of Newtonian fluid and satisfies the relation below:

$$\boldsymbol{T}=\mu\left(\nabla\boldsymbol{U}+(\nabla\boldsymbol{U})^{\mathrm{T}}-\frac{2}{3}(\nabla\cdot\boldsymbol{U})\boldsymbol{I}\right) \tag{4}$$

Here, μ is the average dynamic viscosity with $\mu=\alpha_l\mu_l+\alpha_g\mu_g$; $\boldsymbol{I}$ is the unit tensor.

Equation of state for the gas phase and the liquid phase:

The change of state is assumed to be adiabatic for the gas (shown as equation (5)) in the bubble [12, 24], and the Tait equation (shown as equation (6)), including nonlinear compressibility effects, is used for the liquid phase [25, 26].

$$p\left(\frac{1}{\rho}-\frac{\beta}{\rho_n}\right)^{\gamma_g}=const \tag{5}$$

$$p(\rho)=(p_\infty+B)\left(\frac{\rho}{\rho_\infty}\right)^{n_T}-B \tag{6}$$

Here, ρ_n is the density of the gas phase at normal conditions; β denotes the co-volume dedimensionalized with the molar volume at equilibrium; γ_g denotes the ratio of specific heats; p_∞ is the atmospheric pressure; ρ_∞ is the equilibrium density; n_T is the tait exponent; B is tait pressure.

VOF equation:

For the VOF method [27, 28], only one transport equation (7) for the volume fraction α_l is solved, which is derived from the continuity equation for the liquid (equation (2)).

$$\frac{\partial \alpha_l}{\partial t}+\nabla\cdot\left(\alpha_l \boldsymbol{U}\right)+\nabla\cdot\left(\boldsymbol{U}_{\mathbf{r}}\alpha_l(1-\alpha_l)\right)=\alpha_l(1-\alpha_l)\left(\frac{1}{\rho_g}\frac{d\rho_g}{dt}-\frac{1}{\rho_l}\frac{d\rho_l}{dt}\right)+\alpha_l\nabla\cdot\boldsymbol{U} \tag{7}$$

Here, the third term on the left side of (7) is an artificial term, which is referred as 'counter gradient' transport by Weller [29] and enables interface compression with a numerical compression scheme. The term is only active in the interface region due to the presence of $\alpha_l\alpha_g$ and does not affect the solution outside this region. $\boldsymbol{U}r$ is the relative velocity of the two phases and is determined by equation (8), designated as the 'compression velocity'. Equation (7) is solved by the multidimensional universal limiter with explicit solution (MULES) solver in OpenFOAM [30-31].

$$\boldsymbol{U}_{\boldsymbol{r}}=\min\left[\boldsymbol{C}_{\alpha}\frac{|\phi_f|}{|\boldsymbol{S}_f|},\max\left(\frac{|\phi_f|}{|\boldsymbol{S}_f|}\right)\right]\bullet\frac{\nabla\alpha_{\boldsymbol{l}}}{|\nabla\alpha_{\boldsymbol{l}}+\delta_{\boldsymbol{n}}|}\bullet\boldsymbol{S}_f \tag{8}$$

Here, $\boldsymbol{S}_f$ is the surface area vector; ϕ_f is face volume flux; $\nabla\alpha_l/|\nabla\alpha_l|$ is the normal vector on the interface; δ_{n} is a small number to ensure it's not divided by zero for the outside of the interface region. $\boldsymbol{C}_{\alpha}$ is a user-specified value, which controls the compression of the interface. $\boldsymbol{C}_{\alpha}$=0 corresponds to no compression, $\boldsymbol{C}_{\alpha}$<1 denotes a moderate compression and $\boldsymbol{C}_{\alpha}$>1 denotes an enhanced compression. $\boldsymbol{C}_{\alpha}$ =1 corresponds to conservative compression and is used in this paper.

Coupling LS and VOF:

An algorithm for coupling LS and VOF employed to take the advantages of both the mass conservation of the VOF method and the sharp interface capturing of LS method. Here, a new Level Set field ϕ, which is a signed distance function to distinguish two fluids with a positive value in the liquid phase and a negative value in the gas phase. The interface position is defined by the iso-line ϕ=0. In CLSVOF, only the volume fraction equation (equation (7)) is solved [23]. The initial value for the LS function is obtained from the volume fraction (α) filed and the interface position is defined at the iso-line contour α = 0.5, as below:

$$\phi_0=(2\alpha-1)\Gamma \tag{9}$$

Here, Γ is a small non-dimensional number, which is defined as Γ=0.75Δx; Δx is the mesh cell size, which is the minimum absolute value between the mesh cell center and the mesh cell face center for the nonhomogeneous structured grid.

The LS function is re-distanced by solving the re-initialization equation [23, 32], as below:

$$\begin{aligned}&\frac{\partial\phi}{\partial\tau}=\boldsymbol{S}(\phi_0)(1-\nabla\phi)\\&\phi(\boldsymbol{x},0)=\phi_0(\boldsymbol{x})\end{aligned} \tag{10}$$

Here, τ is the artificial time step and is set as τ =0.1Δx for avoiding sharp changes in the LS function during the reinitialization. $\boldsymbol{x}$ is the position vector; S(ϕ_0) is a sign function.

The surface tension $\boldsymbol{F}_{\sigma}$ is corrected by ϕ as below:

$$\boldsymbol{F}_{\sigma} = \sigma\kappa(\phi)\delta(\phi)\nabla\phi \tag{11}$$

Here, $\kappa(\phi)$ is interface curvature with $\kappa(\phi)= \nabla\cdot\boldsymbol{n}$. $\boldsymbol{n}$ is the normal vector on the interface with $\boldsymbol{n} = \nabla\phi/|\nabla\phi|$, which is accurately obtained due to the LS function is a continuous function. Hence, the interface curvature ($\kappa(\phi)$) is more precise and smoother. δ is the Dirac function to limit the influence of surface tension within the interface and uses a zero value in both fluids as below:

$$\delta(\phi) = \begin{cases} 0 & \textbf{if } |\phi| > \varepsilon \\ \dfrac{1}{2\varepsilon}\left(1+\cos\left(\dfrac{\pi\phi}{\varepsilon}\right)\right) & \textbf{if } |\phi| \le \varepsilon \end{cases} \tag{12}$$

Here, ε is the interface thickness with $\varepsilon = 1.5\Delta x$.
Finally, the physical properties can be calculated using the Heaviside function:

$$H(\phi) = \begin{cases} 0 & \text{if}\phi < -\varepsilon \\ \dfrac{1}{2}\left[1+\dfrac{\phi}{\varepsilon}+\dfrac{1}{\pi}\sin\left(\dfrac{\pi\phi}{\varepsilon}\right)\right] & \text{if } |\phi| \le \varepsilon \\ 1 & \text{if}\phi > \varepsilon \end{cases} \tag{13}$$

A simple sketch of the algorithm is given below:

1. Initialize velocity, pressure and α fields. Meanwhile update density and viscosity.
2. The ϕ, δ and H are initialized from the initial α.
3. Solve equation (7) to obtain a new α value.
4. Update density and viscosity and compute the interface curvature with α value.
5. Reconstruct ϕ (equation (9)) and compute δ (equation (12)) and H (equation (13)) from α value.
6. Recalculate the new surface force using (equation (11)).
7. Create velocity matrix.
8. Solve pressure equation.
9. Calculate the density of each phase from (equation (5)) and (equation (6)).
10. Update the average density.

3. Numerical setup for the initial conditions

As shown in figure 1, a 2D axisymmetric computational region is used in this paper to reduce computational cost. The 2D computational region is meshed with an O-grid type mesh strategy by ICEM in ANSYS, with local refinement in the area of interest; i.e., the region inside and surrounding the cavitation bubble (the red area in figure 1). The total amount of the cells is 1588473, and the minimum cell edge length in *x*-direction is 0.09μm to capture the bubble contours with adequate resolution. The No-slip boundary condition is used for the infinite boundary. The acceleration of gravity is ignored in this paper due to its effect is small for the size and lifetime of the bubble calculated.

The following parameters for the gas and the liquid are used: ρ_l = 998.2kg/m^3; ρ_g = 1.0kg/m^3; μ_l=9.982×10^{-4} pa·s; μ_g=1.589×10^{-5} pa·s; σ=0.07 N/m; ρ_n =1.228 kg/m^3; β=0.00154; γ_g=1.4; p_∞ = 101325 Pa; ρ_∞ = 998.2 kg/m3; n_T = 7.15; B = 3.046×10^8 Pa. The equations are discretized and solved in

OpenFOAM, and the coupling of pressure and velocity is implemented by the pressure-implicit with splitting of operators (PISO) algorithm. An adjustable time-step is used to make the computation more efficient. The maximum Courant number (maxCo) is less than 0.4 to avoid distortion of the interface. An implicit Euler scheme is used for discretizing the transient terms. The TVD scheme with van Leer limiter is used for the spatial discretization. The whole process of computing is executed with 16 CPU cores at 2.10 GHz with 64 GB RAM.

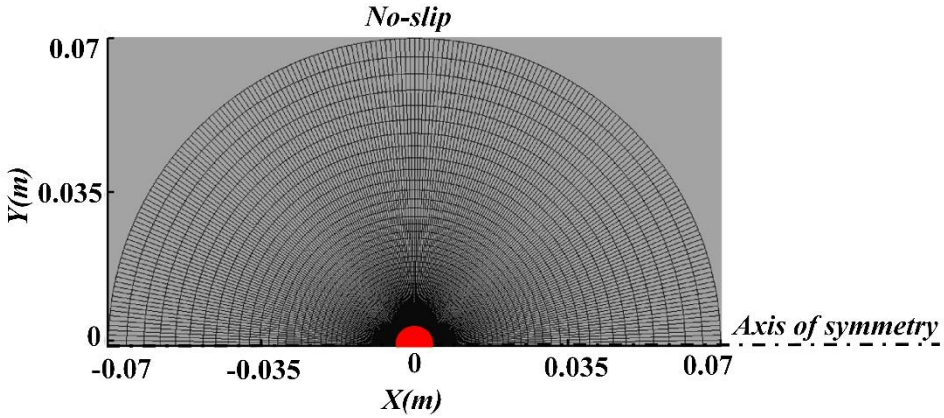

Figure 1. Computational region and the initial boundary conditions.

4. Numerical validation and analysis

The variation of bubble radius with time during the collapse, the rebound and the second collapse are calculated by the Gilmore model, the VOF method and the CLSVOF method, respectively. The numerical simulation results are shown in figure 2 and compared with the experimental results [16, 33]. According to the available experimental data, the initial radius is set as the bubble radius at the beginning of the bubble collapse, where R_{max}=747μm. The initial internal pressure of the bubble is 10pa. In figure 2, it should be noted that the numerical simulation results predicted by the Gilmore model, the VOF method and the CLSVOF method show a little earlier collapse than the experimental results, and the relative error of the first collapse time are 1.38%, 1.95% and 1.37%, respectively. The bubble radius predicted by the VOF method is higher than the experimental results during the bubble rebound, and the relative error of the second maximum radius is 5.63%. In contrast, the results predicted by CLSVOF agree well with the experimental results, in the first collapse, the first rebound, the second collapse and even in the second rebound.

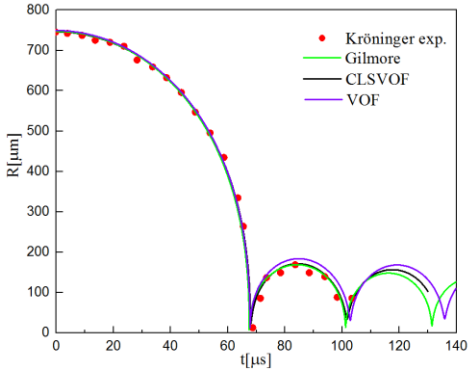

Figure 2. The variation of the bubble radius with time predicted by the Gilmore model, the VOF method and the CLSVOF method and the experimental results [16, 33]. The red dot (●) denotes the experimental data, the green line (—) denotes the results obtained by Gilmore, the black line (—) denotes the results obtained by the CLSVOF and the purple line (—) denotes the results obtained by VOF.

figure 3 shows the detailed pressure and velocity around the cavitation bubble during the first collapse and the first rebound. As shown in figure 3(a) (t=67.9μs), before reaching its minimum radius in infinite field, the bubble keeps collapsing spherically and a local high pressure locates around the cavitation bubble. The value of pressure around the bubble is 20.0Mpa, and the velocity of the bubble wall is about 391.5m/s. At about 68.0μs, the collapse bubble rebounds (see black arrow in figure 3(b)) after reaching its minimum radius and a spherically symmetrical shock wave is emitted with the maximum value of the pressure 430.3Mpa, which arises from the compression of the incondensable gases inside the bubble overcoming the high pressure in the liquid around the bubble in the final collapse stage [34]. The velocity of the bubble wall is uneven and its maximum value (about 206.7m/s) appears on both sides. Later on, the shock wave propagates outside into the liquid and its value of pressure decreases continuously (see (c) and (d) in figure 3).

For detailed investigation on the shock wave, figure 4 shows the emission and the propagation of the shock wave from the cavitation bubble collapse by numerical schlieren method [35]. The black line of the center area represents the wall of the cavitation bubble contour (α_l=0.5 iso-contour). There exist some weaker shock waves surrounding the cavitation bubble (see figure 4 (b), (c) and (d)), meaning a series of shock waves are emitted during the bubble rebound. The loss of energy due to the emission of shock waves leads to smaller radius of the second growth bubble than the first growth bubble (see figure 2). Supponen et al. [34] also found that the most energetic shock wave are emitted by highly spherical collapse, reaching up to about 90% of the initial bubble energy.

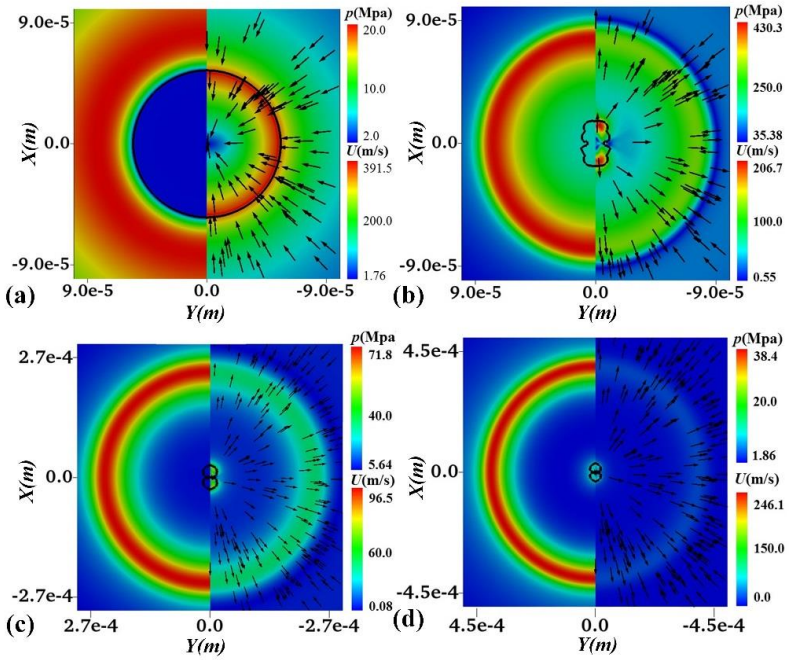

Figure 3. The detailed description for pressure and velocity field during the bubble first collapse and first rebound at times t =67.9μs (a), 68.0μs (b), 68.1μs (c) and 68.2μs (d), respectively.

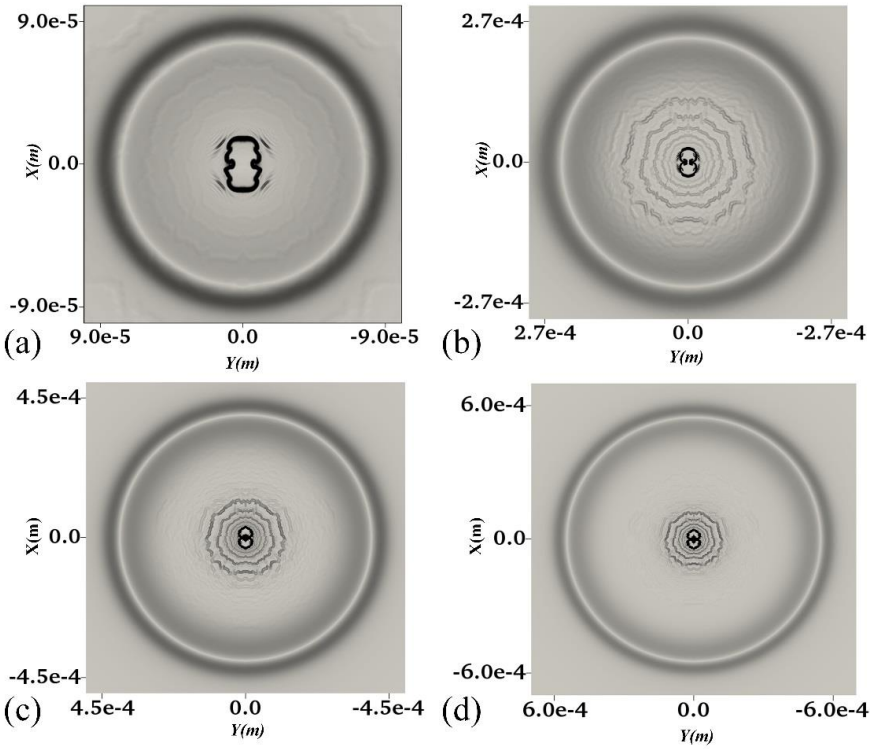

Figure 4. The propagation of the shock wave after cavitation bubble collapse by numerical schlieren method at 68.0μs (a), 68.1μs (b), 68.2μs (c) and 68.3μs (d).

5. Conclusion

To improve the accuracy of the simulation of the interface curvature and surface tension force, a coupled level set (LS) and volume of fluid (VOF) method is employed to track the movement of the gas-liquid interface, based on the open source software OpenFOAM. Compared with the VOF method, the bubble radius during the bubble collapse and rebound predicted by the CLSVOF method are more consistent with the experimental results. So, it's very clear that the gas-liquid interface curvature and the surface tension force computations are well improved by coupling level set and volume of fluid method. The results of the CLSVOF method also illustrate the emission of the strong shock wave when the collapse bubble reaches its minimum radius, and then many weaker shock waves are emitted during the bubble rebound.

Acknowledgements

The authors would like to acknowledge the supports of the National Natural Science Foundation of China (Project No. 51606221), the Science Foundation of China University of Petroleum, Beijing (No. 2462016YJRC003).

References

[1] Zhu Z F and Fang S L 2012 Numerical investigation of cavitation performance of ship

propellers. *J. Hydrodyn.* B **24** 347-353

[2] Shengcai L 2006 Cavitation enhancement of silt erosion—an envisaged micro model. *Wear.* **260** 1145-50

[3] Kim D J, Sung H J, Choi C H and Kim J S 2017 Cavitation instabilities of an inducer in a cryogenic pump. *Acta Astronautica*. **132** 19-24

[4] Rayleigh L 1917 On the pressure developed in a liquid during the collapse of a spherical cavity. *The London, Edinburgh, and Dublin Philosophical Magazine and Journal of Science*. **34** 94–98

[5] Plesset M S and Prosperetti A 1977 Bubble dynamics and cavitation. *Annu Rev Fluid Mech*. **9** 145-185

[6] Gilmore F R 1952 The growth or collapse of a spherical bubble in a viscous compressible liquid

[7] Blake J R, Hooton M C, Robinson P B and Tong R P 1997 Collapsing cavities, toroidal bubbles and jet impact. *Philosophical Transactions of the Royal Society of London A: Mathematical, Physical and Engineering Sciences*. **355** 537-550

[8] Blake J R, Taib B B and Doherty G 1986 Transient cavities near boundaries. Part 1. Rigid boundary. *J. Fluid Mech.* **170** 479-497

[9] Brujan E A, Keen G S, Vogel A and Blake J R 2002 The final stage of the collapse of a cavitation bubble close to a rigid boundary. *Phys. Fluids.* **14** 85-92

[10] Wang Q X 2014 Multi-oscillations of a bubble in a compressible liquid near a rigid boundary. *J. Fluid Mech.* **745** 509-536

[11] Christian C M 2012 *Modeling Laser-Generated Cavitation Bubbles*

[12] Koch, M., Lechner, C., Reuter, F., Köhler, K., Mettin, R., & Lauterborn, W. (2016). Numerical modeling of laser generated cavitation bubbles with the finite volume and volume of fluid method, using OpenFOAM. *Comput. Fluids.* **126** 71-90

[13] Lechner C, Koch M, Lauterborn W and Mettin R 2017 Pressure and tension waves from bubble collapse near a solid boundary: A numerical approach. *J. Acoust. Soc. Am.* **142** 3649-59

[14] Han B, Köhler K, Jungnickel K, Mettin R, Lauterborn W and Vogel A 2015 Dynamics of laser induced bubble pairs. *J Fluid Mech*. **771** 706-742.

[15] Han R, Li S, Zhang A M and Wang Q X 2016 Modelling for three dimensional coalescence of two bubbles. *Phys. Fluids*. **28** 062104

[16] Müller S, Bachmann M, Kröninger D, Kurz T and Helluy P 2009 Comparison and validation of compressible flow simulations of laser-induced cavitation bubbles. *Comput. Fluids*. **38** 1850-62

[17] Sethian J A and Smereka P 2003 Level set methods for fluid interfaces. *Annu rev fluid mech*. **35** 341-372

[18] Hirt C W and Nichols B D 1981 Volume of fluid (VOF) method for the dynamics of free boundaries. *J Comput Phys*. **39** 201-225

[19] Sussman M, Smereka P and Osher S 1994 A level set approach for computing solutions to incompressible two-phase flow. *J Comput Phys*. **114** 146-159

[20] Sussman M 2003 A second order coupled level set and volume-of-fluid method for computing growth and collapse of vapor bubbles. *J Comput Phys*. **187** 110-136

[21] Jasak H The OpenFOAM Extend Project (Community-driven Releases of Open-FOAM)

[22] Li T, Wang S, Li S and Zhang A M 2018 Numerical investigation of an underwater explosion bubble based on FVM and VOF. *Appl Ocean Res*. **74** 49-58
[23] Albadawi A, Donoghue D B, Robinson A J, Murray D B and Delauré Y M C 2013 Influence of surface tension implementation in volume of fluid and coupled volume of fluid with level set methods for bubble growth and detachment. *Int J Multiphas Flow*. **53** 11-28
[24] Löfstedt R, Barber B P and Putterman S J 1993 Toward a hydrodynamic theory of sonoluminescence. *Phys. Fluids*. **5** 2911-28
[25] Fujikawa S and Akamatsu T 1980 Effects of the non-equilibrium condensation of vapour on the pressure wave produced by the collapse of a bubble in a liquid. *J Fluid Mech*. **97** 481-512
[26] Koukouvinis P, Gavaises M, Supponen O and Farhat M 2016 Simulation of bubble expansion and collapse in the vicinity of a free surface. *Phys. Fluids*. **28** 052103
[27] Brackbill J U, Kothe D B and Zemach C 1992 A continuum method for modeling surface tension. *J Comput Phys*. **100** 335-354
[28] Deshpande S S, Anumolu L and Trujillo M F 2012 Evaluating the performance of the two-phase flow solver interFoam. *Computational science & discovery*. **5** 014016
[29] Weller H G 2008 A new approach to VOF-based interface capturing methods for incompressible and compressible flow. *OpenCFD Ltd. Report TR/HGW/04*
[30] Greenshields C J 2015 *Openfoam user guide*. OpenFOAM Foundation Ltd version 3
[31] Zalesak S T 1979 Fully multidimensional flux-corrected transport algorithms for fluids. *J Comput Phys*. **31** 335-362
[32] Haghshenas M, Wilson J A and Kumar R 2017 Algebraic coupled level set-volume of fluid method for surface tension dominant two-phase flows. *Int J Multiphas Flow*. **90** 13-28
[33] Kröninger D 2008 *Particle-tracking-velocimetry-Messungen an kollabierenden Kavitationsblasen*. Doktorarbeit, Drittes Physikalisches Institut, Universität Göttingen. 6
[34] Supponen O, Obreschkow D, Kobel P, Tinguely M, Dorsaz N and Farhat M 2017 Shock waves from nonspherical cavitation bubbles. *Phys Rev Fluids*. **2** 093601
[35] Settles G S 2012 *Schlieren and shadowgraph techniques: visualizing phenomena in transparent media*. Springer Science & Business Media